chemosensors

Article

Flexible Humidity Sensor Based on Chemically Reduced Graphene Oxide

Anna Maria Laera *, Gennaro Cassano, Emiliano Burresi, Maria Lucia Protopapa and Michele Penza

ENEA-Italian National Agency for New Technologies, Energy and Sustainable Economic Development, Brindisi Research Centre, S.S. 7, Km. 706, 72100 Brindisi, Italy; gennaro.cassano@enea.it (G.C.); emiliano.burresi@enea.it (E.B.); lucia.protopapa@enea.it (M.L.P.); michele.penza@enea.it (M.P.)
* Correspondence: annamaria.laera@enea.it; Tel.: +39-0831201588

Abstract: The accurate measurement of moisture content in pure gases and in gas mixtures, such as air, has great relevance in many industrial processes. In the present study, graphene oxide reduced through a mild alkaline treatment was used as a humidity sensing material to fabricate a flexible chemiresistive device operating at room temperature. The active layer was deposited by solution casting on a substrate of bimatted polyester, previously coated with inkjet-printed interdigitated electrodes made of silver. Structural investigations were performed by means of X-ray diffraction, Raman spectroscopy, and FTIR spectroscopy, while the optical properties were investigated using UV-VIS absorption and photoluminescence excitation spectroscopy. With increasing relative humidity from 0 to 80%, the electrical resistance decreased from about 1.4 GΩ to 2.5 MΩ. The extraordinarily large range of resistance values highlights the ultrahigh humidity sensitivity of re-duced graphene oxide, which acquires a fair amount of electrical conductivity after physisorption of water molecules but results in a highly resistive material in dry air. The high sensitivity at room temperature, the response's repeatability, the wide relative humidity range detected, and the fast response time are the main advantages of the proposed humidity sensor, while the presence of some hysteresis, mainly at low relative humidity, and the recovery time need further improve-ment. Finally, the sensing mechanisms are briefly discussed.

Keywords: graphene oxide; humidity sensors; chemiresistive sensors; interdigitated electrodes; flexible electronics

Citation: Laera, A.M.; Cassano, G.; Burresi, E.; Protopapa, M.L.; Penza, M. Flexible Humidity Sensor Based on Chemically Reduced Graphene Oxide. *Chemosensors* **2024**, *12*, 245. https://doi.org/10.3390/chemosensors12120245

Received: 9 October 2024
Revised: 19 November 2024
Accepted: 20 November 2024
Published: 22 November 2024

1. Introduction

Humidity monitoring and control have a crucial impact on many different fields, such as agriculture, meteorology, the production and manufacturing of microelectronics, medicines, textiles, and foods, as well as the heating, ventilation, and air conditioning (HVAC) industry. For instance, high levels of relative humidity (RH) can decrease the shelf life of fruit and vegetables and can promote bacterial growth and spoilage in several food products, while low humidity can cause some foods to dry out and lose flavor. In the semiconductor and electronics industries, incorrect humidity control can compromise the safety of the work environment and can damage various sensitive components and integrated circuits. In addition, the measurement of humidity has great relevance in newly emerging areas, including breath analysis for dis-ease diagnosis, structural health monitoring, the development of robotic smart skin, the Internet of Things (IoT), and the design of wearable devices [1]. Many types of humidity sensors have been proposed to satisfy this large variety of applications and requirements [2]. Depending on the physical properties involved in the sensing mechanism, the humidity sensor can be classified as electrical, electrochemical, capacitive, gravimetric, optical, or field effect transistor (FET).

Materials with two-dimensional (2D) morphology have been considered for humidity sensing due to their advantageous features, such as the large specific surface area, mechanical robustness, and the electronic structure that is tunable through the scaling down of size

from bulk to a few layers [3]. In addition, planar geometry and mechanical flexibility make the 2D materials suitable candidates for the fabrication of wearable devices. Among 2D materials, graphene oxide (GO) has been particularly investigated for its solution-processing compatibility and its hydrophilic nature, both of which are attributed to its high content of oxygenated functional groups, including epoxide (C−O−C) and hydroxyl (−OH)—located mainly on the interior of the sheets—as well as carboxyl (−COOH) and carbonyl (−C−OH), located mainly on the edges [4,5]. GO has also become an attractive material for gas sensing applications for its low cost, environmental friendliness, light weight, ease of synthesis and surface functionalization, and for its electrical properties that are tunable via many reduction methods. In the last twenty years, GO's exceptional sensitivity to-wards water has been demonstrated in numerous different devices, such as quartz crystal microbalances (QCM) [6–8], as well as surface acoustic wave (SAW) [9,10], capacitive [11], piezoresistive [12] and electrical sensors [13,14]. Furthermore, GO's outstanding hydrophilicity has allowed for the design of efficient, self-powered humidity sensors able to operate in remote settings without an external power source [15,16].

Among electrical devices, chemiresistive sensors with an interdigitated electrode geometry generally provide repeatable output signals with excellent stability and reliability over a long period. The operating principle of chemiresistors is based on the changes in electrical resistance in sensing layers upon chemical interaction with analytes. In GO-based chemiresistive devices, a decrease in electrical resistance was generally observed with increasing %RH, but surprisingly, in some cases, an opposite trend was reported [17,18]. The inconsistencies between published data have not been deeply understood because the complex structure of GO, which can present variable stoichiometry, makes the sensing mechanism more complicated compared to other conventional materials. Discrepancies in gas sensing behaviors can be attributed to many factors, including differences in device structure and in film topology and morphology. Different thin film topologies were described depending on either the selected deposition method or thickness. Disordered and rough films with extended wrinkles are commonly observed due to the flexible nature of GO layers, which can easily fold or crumple during deposition [19]. Both surface ad-sorption and interlayer swelling impact electrical conductivity when water molecules diffuse between the 2D sheets of the stacked structure. Fully understanding the role of all factors involved in water sensing, such as structure, morphology, and oxidation grade, will be crucial to improving the performance of GO-based devices.

An excessive oxidation grade makes GO an insulating material; in consequence, chemical, thermal and photo-thermal methods have been commonly employed to pro-duce reduced GO (rGO) with different carbon-to-oxygen ratios [20]. During the reduc-tion process, the carbon-to-oxygen ratio increases due to the partial restoration of the graphitic network. GO thermal reduction can be accompanied by a release of CO and CO_2, and the carbon loss can produce voids and defects in the rGO honeycomb structure [5,21]. Among the different chemical methods, reduction using hydrazine is largely employed to remove oxygen functional groups without removing carbon atoms; as a result, the GO layers can be almost totally preserved. However, hydrazine is a highly toxic, flammable, and explosive reagent, and the incorporation of nitrogen has been observed in hydrazine-treated GO [19]. Sodio borohydride and its derivatives [22], oxalic acid [23], and sodium hydrosulfite [24] are further examples of reducing substances widely employed for GO chemical reduction. Interestingly, the deoxygenation of GO was also observed in alkaline solutions even though the underlying mechanism has not been fully understood [25].

In the present study, GO obtained using a modified Hummers' method was partially reduced under mild conditions by an alkaline treatment in a water solution of KOH [26]. Compared to the usual reducing substances, KOH is less effective but has the advantage of allowing both the improvement of electrical conductivity and the preservation of more oxygenated functional groups, which are the major adsorption sites for water molecules. The reduction method of using an alkaline water solution provides an alternative green route useful for the elimination of hazardous reducing compounds. A flexible

chemiresistive sensor operating at room temperature was fabricated by drop casting an rGO water solution on a substrate of bimatted polyester that was previously coated with inkjet-printed interdigitated electrodes made of silver. The produced device showed high sensitivity in the RH range of 10–80%. The performance of the rGO-based sensor was also investigated considering factors beyond sensitivity, including response and recovery time, hysteresis, and reliability, with the aim of furnishing useful information regarding the effect of chemical reduction with KOH on rGO sensing properties. The chemical treatment in alkaline solution allowed for either avoiding the use of hazardous reducing agents or preserving many oxygenated functionalities on the rGO surface. Controlling the structure, chemical stability, and properties of rGO by choosing the suitable procedure for synthesis and chemical reduction will be crucial to designing reliable humidity sensors able to operate in real time at room temperature and easily integrate into wearable equipment. Finally, the remarkable sensitivity, the response repeatability at room temperature, the wide RH range detected, and the fast recovery time are the main advantages of the proposed humidity sensor.

2. Materials and Methods

2.1. GO Synthesis and Characterization

All the reagents employed for GO synthesis were purchased from Sigma-Aldrich (St. Louis, MO, USA) and used without further purification. Following a modified Hammer's method [27], an aqueous solution of H_2SO_4 at 96% in weight (23 mL) was added in a flask containing commercial graphite (1 g). An ice bath was used to cool down the graphite suspension and little aliquots of $KMnO_4$ (3 g) were slowly added under vigorous stirring. After removal of the ice bath, the excess of $KMnO_4$ was neutralized by gradually pouring a diluted solution of H_2O_2 (10 mL) in water (140 mL) at room temperature. The produced GO brown-yellowish powder was separated by centrifugation (4000 rpm for 10 min) and was washed three times by using a water solution of HCl with a volume concentration of 10%.

Finally, an alkaline treatment was performed dispersing the GO powder (100 mg) in a water solution of KOH (10 mL at 10% in weight) at room temperature.

Optical properties of rGO were investigated in water solutions by using a Cary 5000 UV-Vis-NIR spectrophotometer supplied by Agilent Technologies (Leini, TO, Italy) and a FluroMax-4 spectrophotometer supplied by Horiba Scientific (Roma, Italy).

The rGO dried powder was compressed into KBr pellets to acquire FTIR spectra with a Nicolet^{TM} iS50 spectrometer furnished by Thermo Fischer Scientific (Rodano, MI, Italy). All spectra were recorded after 64 scans from 4000 to 400 cm^{-1}.

GO Raman spectra were carried out on SiO_2 substrates by means of the Raman spectrometer LabRam HR Evolution by Horiba Scientific (Roma, Italy), equipped with a continuous laser source of wavelength 633 nm. The beam was focused on the sample using the 100× objective with a diameter of about 2 μm, selecting a maximum power of 17 mW and an integration time of 1 s.

X-ray diffraction analysis was carried out by means of the Multipurpose Empyrean (Panalytical, Almelo, The Netherlands) diffractometer equipped with a Cu anode (Kα1 = 1.540596 Å). The incident X-ray beam was collimated through a PDS prefix module with a Soller slit (0.04 mm) and a divergence slit (1/2°), while a Soller slit (0.04 mm) and an antiscatter slit (7 mm) were placed in front of the detector. The samples were loaded on a powder sample stage in spinning active mode. A 2D solid-state hybrid pix-el (PIXcel3D) was used as the detector.

2.2. Chemiresistive Device Fabrication and Experimental Setup for Gas Sensing Measurements

The chemiresistive device was fabricated aligning the sheets of bimatted polyester under a photomask, previously impressed by screen printing with a bromograph. A silver based conductive ink was applied and cured at high temperature to produce interdigitated electrodes with line and span width of 1 mm. Each electrode, made of 4 lines distributed on a total area of 16 × 19 mm, was coated with an active layer of rGO by drop casting with

a micropipette of a water solution having a concentration of 2 mg/mL. The deposited rGO film was dried on a hot plate at 100 °C for about an hour.

The obtained sensor was placed in a sealed stainless cell with a volume of approximately 500 cc and in order to stabilize the electrical resistance values, a constant flow of dry air was applied for a few hours. The complete measurement setup was schematized in Figure 1.

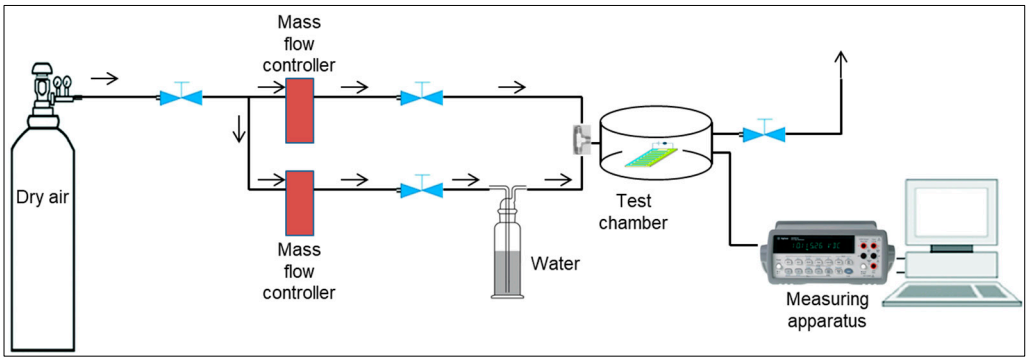

Figure 1. Schematic of measurement setup.

The introduction of humidity into the test chamber was performed by passing a controlled flow of a carrier gas (dry air) through a glass cylinder containing water at room temperature. An additional dry air stream was used to control the dilution of the saturated stream, keeping the total flow rate at 1000 sccm. The two flow rates were tuned by using distinct mass flowmeters supplied by MKS Instruments (Berlin, Germany) and controlled by the REIN managing program (AETHIA, Colleretto Giacosa, TO, Italy). The electrical resistance values were recorded for varying RH in the range from 7% to 80% by the volt-amperometric technique in the two-pole format by the multimeter Agilent 34411A (Cernusco sul Naviglio, MI, Italy). The chemiresistive sensor was automatically scanned by a switch system, the Keithley 7001, equipped with a low-current Keithley 7158 scanner card with a multiplexing read-out (Keithley Instruments, Settimo Milanese, MI, Italy). All data were acquired and stored in a PC-based workstation equipped with software compiled in Agilent-VEE using an USB-GPIB interface-card Agilent-82357A (Cernusco sul Naviglio, MI, Italy). The RH values were monitored by using a Vaisala humidity and temperature probe (Vantaa, Finland). All the exposures to wet air were conducted at room temperature with a sensing cycle composed by the following three steps: (i) a period of 60 min with dry air flow to reach a stable value of resistance; (ii) an exposure time of 10 min to various RH values; and finally, (iii) a recovery time of 50 min under dry air flow until restoring the initial value of resistance.

Analogous sensing cycles were performed for VOCs exposures during which an Owlstone OHG-4 humidity generator (Boston, MA, USA) was used to produce a stable concentration of 50% RH.

As important indicator of device performance, the sensor responses SR% were calculated with the following formula

$$SR(\%) = \left(\frac{R_{dry} - R_{wet}}{R_{dry}} \right) \times 100 \quad (1)$$

where R_{dry} is the electrical resistance measured in dry air and R_{wet} is the electrical resistance measured upon exposure to wet air. At least three exposure cycles were performed for each considered value of %RH, and the average values of the related SR(%) were calculated. The relative standard deviation for each group of measurements was less than 10%.

The sensor sensitivity S, defined as the sensor response per unit increase in %RH, was calculated by applying the equation [28]:

$$S = \left(\frac{R_{wet1} - R_{wet2}}{\%RH_2 - \%RH_1} \right) \quad (2)$$

where R_{wet2} and R_{wet1} are the electrical resistance values at relative humidity $\%RH_2$ and $\%RH_1$, respectively.

Moreover, the hysteresis H was evaluated by using the following expression [29,30]:

$$H = \left(\frac{R_D - R_A}{S} \right) \quad (3)$$

where R_D is the electrical resistance measured during the desorption process and R_A is the electrical resistance measured at same value of %RH during the adsorption process.

Response and recovery time were determined considering the required time to reach 90% of the maximum response in wet air and the 10% in dry air, respectively.

3. Results and Discussion

3.1. Material Characterization

The effects of the basic cleavage performed in a water solution of KOH clearly emerged in FTIR spectra reported in Figure 2a,b for pristine GO and rGO respectively. The signal at 1700 cm^{-1}, due to –C=O stretching vibration, decreased in intensity following basic treatment, compared to the peak at 1580 cm^{-1}, ascribed to aromatic stretching vibration of C=C bonds. As expected for a reducing process, new sp^2 carbon atoms were introduced extending the graphene moieties and in consequence the signal at 1580 cm^{-1} became more prominent. However, the adopted mild alkaline treatment allowed to preserve many of oxygenated functionalities as demonstrated by FTIR signals at 1373, 1220 and 1054 cm^{-1} that arise from –C–OH stretching, C–O–C stretching and C–O stretching, respectively. The large band at 3385 cm^{-1} was due either to O–H stretching of hydroxyl groups covalently bonded to GO sheets or adsorbed water.

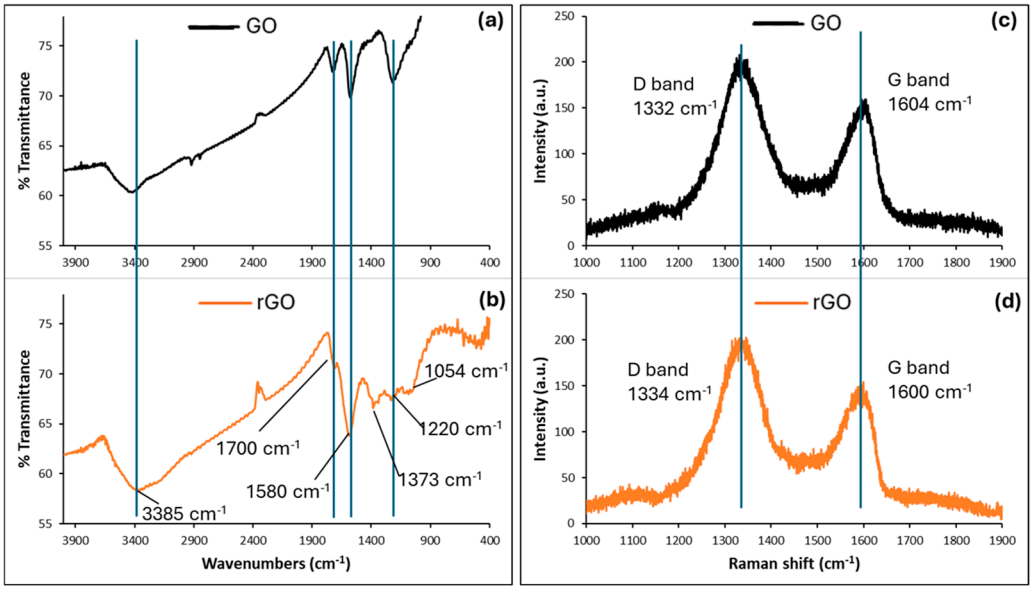

Figure 2. FTIR spectra of GO (**a**) and rGO (**b**) obtained in alkali solution. Raman spectra of GO (**c**) and rGO (**d**) obtained in alkali solution.

In GO Raman spectra, two prominent signals are typically observed, the G band, ubiquitously present in all compounds with honeycomb graphitic structure (sp^2 bonded carbon), and the D band, observable when order and symmetry is broken by defects and

oxygenated functional groups (breathing mode of sp^2 carbon). No noticeable changes emerged in GO and rGO Raman spectra, reported in Figure 2c,d. A slight red shift was observed in G band frequency of rGO (from 1604 to 1600 cm^{-1}) due to the decrease of isolated double bonds that resonate at higher frequencies [31]. The intensities ratio of the D and G bands (I_D/I_G) can be related to the extent of defects on the graphene-based materials. An unchanged I_D/I_G value in rGO Raman spectra respect to pristine GO indicated the similar extent of defects, that were not significantly affected by the chosen mild alkaline treatment. It is worth noting that a reduction process does not necessarily decrease the extent of defects but, on the contrary, can increase it [32].

As is evident in the UV-Vis absorption spectra reported in Figure 3a, higher absorption values at around 265 nm were recorded for the rGO water solution. Consistent with the literature, the π-π^* transition of C=C shifts to higher wavelengths in rGO solutions compared to those of GO, due to the removal of some functional groups on the basal plane and restoration of the con-jugated structure [33].

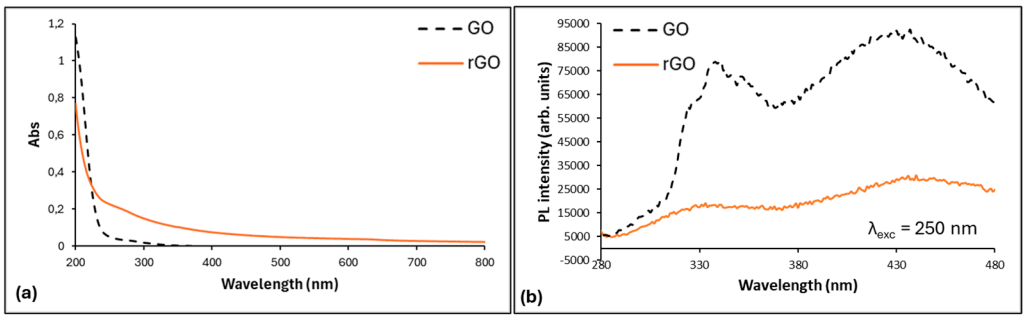

Figure 3. UV-Vis absorption spectra (**a**) and PL spectra (**b**) of GO and rGO in water solutions.

The photoluminescence emission spectra of GO and rGO with an excitation wavelength λ_{exc} of 250 nm were reported in Figure 3b. On GO sheets the oxygenated functional groups are not homogeneously distributed because the aggregation of epoxide and hydroxyl groups in specific strips is energetically favorable as emerged with first-principles calculations [34]. In consequence, the broad emission spectra of pristine GO, centered at 430 nm, can be ascribed to recombination of electron-hole pairs in localized defective states of sp^2 carbon clusters embedded in a matrix of sp^3-hybridized carbon atoms. The localized defective states originate from the large fraction of distorted carbon atoms attached to oxygenated functional groups [35]. A significant quenching of photoluminescence was observed in rGO spectra shown in Figure 3b, due to the decrease of localized defective states because of deoxygenation by reduction. Furthermore, the reduction process usually induces formation of numerous new small sp^2 clusters able to furnish non radiative pathways for carriers' transport by hopping [36].

XRD pattern for rGO slurry was shown in Figure 4.

This sample was obtained from rGO powder after sonication in an ultrasonic bath for 30 minutes. This sonication time is approximately sufficient to dissolve the rGO sheet in water, leading to the loss of the primarily regular arrangement of the atoms in rGO. The increase in atomic disorder is well illustrated in Figure 4, where only two weak reflections (001) and (110) are barely detectable. The (001) reflection (around 12° (2Theta)) indicates that a residual order among stacked parallel sheets, reduced with respect to the GO bulk, persists after sonication; hence, the GO flakes have not been dissolved completely in the solution. The other reflection (110) is even weaker than (001), and it reflects a very slight rearrangement of the at-oms along the sheet plane.

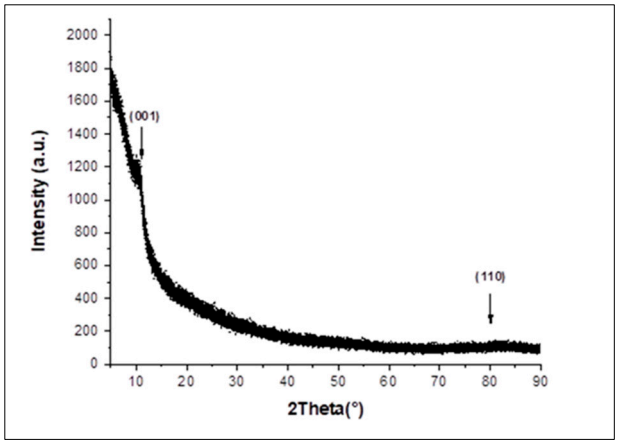

Figure 4. XRD pattern of the rGO sample.

3.2. Sensing Properties and Mechanism Discussion

The sensing properties of rGO were evaluated considering several parameters such as sensor responses, sensitivity, response time and recovery time, hysteresis and repeatability. Typical signals of fabricated rGO-based sensor were reported in Figure 5 for exposure to wet air in the range of 7–80% RH. All measurements cycles were performed at room temperature upon dry air, and an electrical resistance of about 1.4 GΩ was recorded.

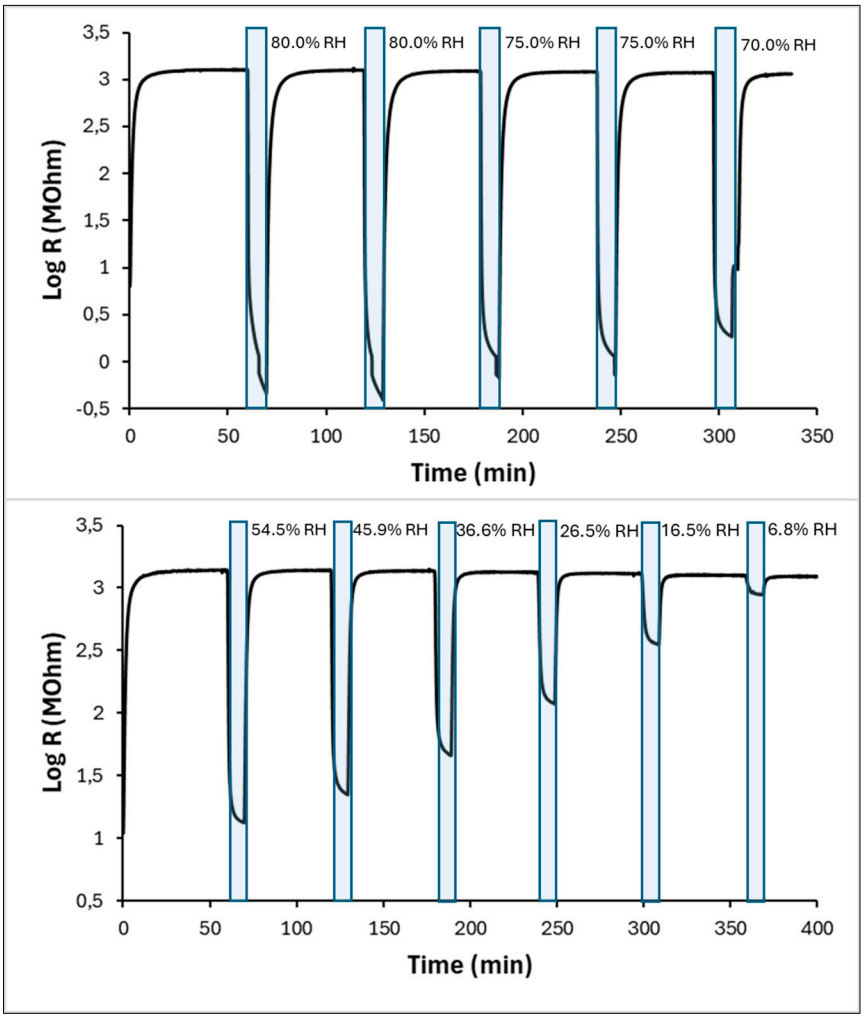

Figure 5. Sensor signals upon exposure to several decreasing %RH values at room temperature.

It is worth noting that pristine not reduced GO showed electrical resistance values in dry air higher than 2.0 GΩ, corresponding to the instrumental limit of our used multimeter. The electrically-insulating character of pristine GO prevents its employment in sensor devices. The proposed treatment in 10% alkaline solution by weight, performed for 15 min at room temperature, resulted sufficient to improve conductivity. Higher concentrations, longer process times and higher temperatures were avoided to preserve a large number of oxygenated functionalities, which are the major adsorption sites for water molecules.

Under exposure to 80% RH the electrical resistance decreased from about 1.4 GΩ to 2.5 MΩ attesting the extraordinary sensitivity of rGO towards humidity. A slight decline of pristine resistance after each exposure cycle was observed, indicating an incomplete removal of water molecules from the sensing layer. The sensor response (SR%), calculated by using expression (1), grew from 29.2% to 99.9% increasing RH from 6.0% to 80.0%.

As shown in Figure 6a, the SR% variation versus humidity can be fitted to a logarithmic correlation function. At values of RH higher than 70%, sensor saturation was observed and sensitivity did not further change, as highlighted in the inset curve in Figure 6a showing an enlarged scale. Higher values of sensitivity S were recorded at low humidity levels and the maximum sensitivity was reached at 17% RH (Figure 6b). In the range of 20–60% RH, a linear increase in sensitivity was found, as shown in the in-set curve of Figure 6b.

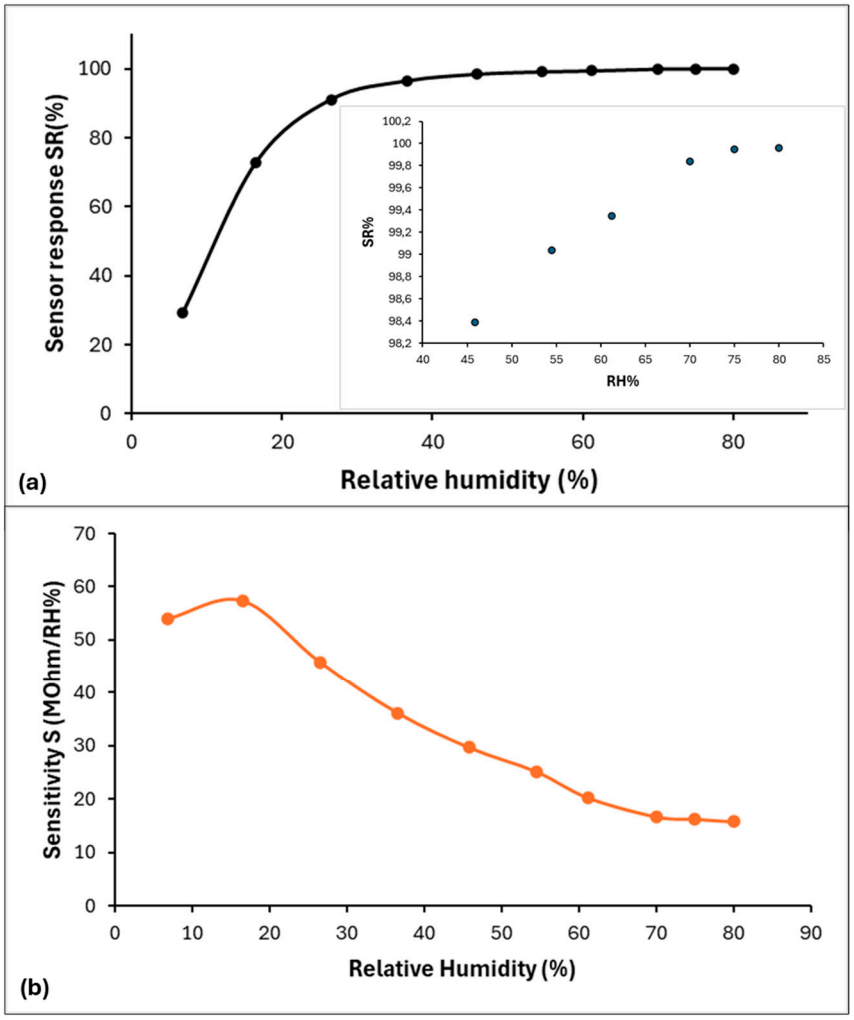

Figure 6. Sensor responses SR% (**a**) and sensor sensitivity S (**b**) versus increasing %RH.

The maximum variation of electrical resistance was observed within the range of 0–40% RH, as highlighted in the diagram in Figure 7, obtained upon exposure to several decreasing and increasing humidity values with stepwise progression. A drastic increase by two orders of magnitude in electrical resistance from about 13.0 MOhm to 1300.0 MOhm was detected by decreasing humidity from 40.3% RH to dry air (Figure 7b). In contrast, Figure 7a demonstrates the changes in electrical resistance in the smallest range of 2.5–13.0 MOhm upon decreasing humidity from 80.9% RH to 50.0% RH. During the absorption process, as shown in Figure 7c,d, the maximum decrease in electrical resistance was similarly observed in the range of 0–37.5% RH.

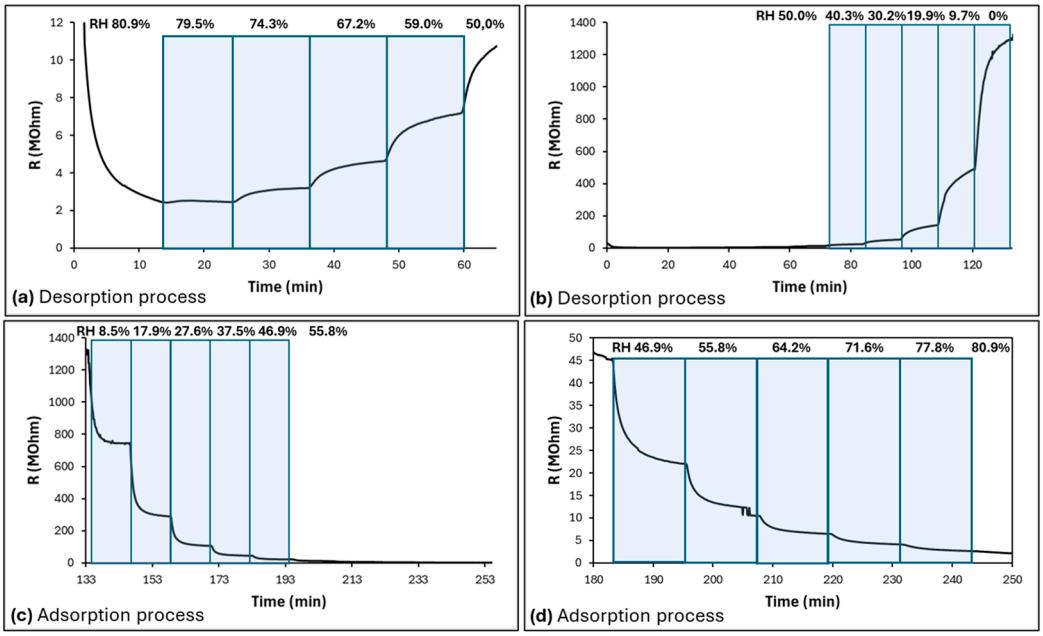

Figure 7. Stepwise diagram of sensor resistance versus time upon exposure to several decreasing %RH values within the range 80.9–50.0% (**a**) and 50.0–0% (**b**) and upon exposure to several increasing %RH values within the range 0–46.9% (**c**) and 46.9–80.9% (**d**).

At low humidity exposure, the sensor performances mainly relied on the surface adhesion since the water molecules primarily interacted with oxygenated groups on rGO layers through the formation of two hydrogen bonds [11]. Thanks to the high hydrophilicity, a first layer of physiosorbed water molecules with low mobility rapidly assembled on rGO surface during adsorption process (Figure 7c). Initially, very high values of electrical resistance were recorded being difficult the hopping transfer of proton between adjacent hydroxyl groups. However, a drastic increase of electrical conductivity rapidly occurred mainly due to the enhancement of ion conduction. With increasing of %RH, the water molecules can interact either with rGO surface or with other adsorbed water molecules arranging in multiple layers in which they preserved great mobility as in liquid state. Cerveny et al. demonstrated that the freer water-water interactions were predominant respect to the bonded water state when the hydration level overcame the 15% in weight [37]. Therefore, the conductivity generated by Grotthuss chain reaction ($H_2O + H_3O^+ \leftrightarrows H_3O^+ + H_2O$) became soon prominent respect to low conductivity of rGO sheets, inducing an outstanding resistance decrease of two orders of magnitude in sensor device. Protons involved in conduction probably arose from hydrolysis of the functional groups present on rGO as suggested by Gao et al. [38]. Recent theoretical studies also demonstrated that the reactive events at rGO interface with water molecules can lead to hydronium formation and to negatively charge the rGO sheets [4,39]. At values of relative humidity higher than 70%, the sensitivity did not further change. In this regime, the water molecules can deeply penetrate inside the inherent layered structure of rGO making sensing performance more complex.

The rGO film should be swollen and the increasing of interlayer distance could negatively affect the resistance values.

The described sensing mechanism remarkably distinguishes the rGO-based humidity sensors from other carbon-based devices, such as graphene-based or carbon nanotube-based humidity sensors, in which electrostatic interactions and charge transfers are mainly involved [40,41].

Additional relevant indicators of device performances, such as the response time and recovery time, were reported in Figure 8a for exposure at 61.0% RH. While the response time became exceptionally fast and required few seconds, the recovery time was, on the contrary, excessively slow, requiring some minutes. These clearly indicate a rapid adsorption process and a delayed desorption process. During desorption the water molecules need to escape the attraction either of the rGO oxygenated functionalities or the other surrounding water molecules in order to detach from the rGO surface.

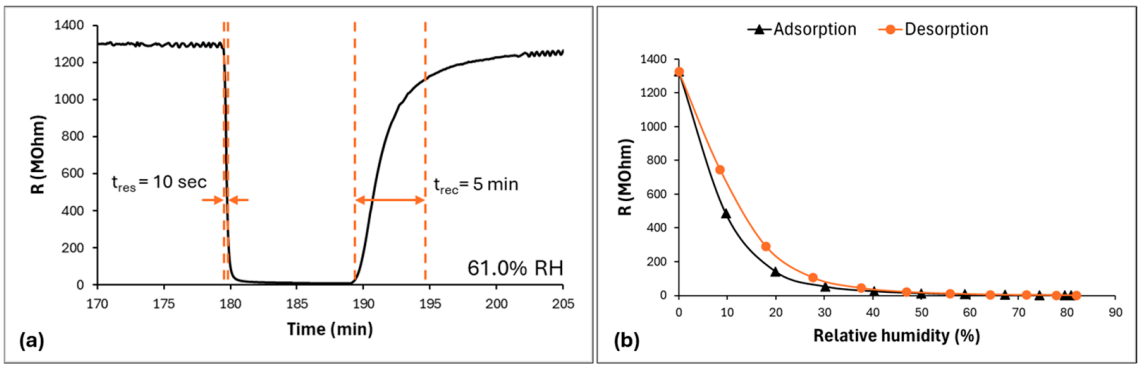

Figure 8. Response and recovery time evaluated for exposure at 61.0% RH (**a**) and hysteresis curve (**b**).

Due to the large difference between adsorption and desorption rate, significant hysteresis effects were observed mainly for low humidity values (Figure 8b).

As previously described, two types of hydrogen bond are involved in sensing mechanism: bonds formed between water molecules and oxygenated functional groups on rGO surface and bonds between water molecules and other water molecules. Below 20% RH, the water molecules are mainly involved in hydrogen bond with rGO surface and during the desorption process (humidity decrement), the detachment of these molecules requires more energy than absorption, causing visible hysteresis. At higher level of %RH, the hysteresis effects become less visible, because the absorption and desorption processes of water molecules bonded to other water molecules require similar energy. The adsorption and desorption curves in Figure 8b were fitted with exponential functions and the maximum hysteresis of the sensor, calculated according to Equation (3), resulted as 8.8%. This high hysteresis value can be also explained by considering the deep diffusion of water molecules among rGO layers (with a residual stacking order having interlayer distance approximately about 0.7 nm as the XRD pattern showed) which cannot be totally removed, as also highlighted considering the slight reduction of pristine electrical resistance in Figure 5.

Table 1 represents a comparison of sensing characteristics of previously reported works focused on electrical sensors in which measurements of resistance or impedance were performed. In few cases not reduced GO was used, due to its very low electrical conductivity. Although the gas test conditions can remarkably vary from publication to publication, a significant hysteresis was often measured being the main drawback in rGO-based electrical sensors.

Table 1. Humidity sensor performance of this work compared with the literature.

GO Reduction Method	Measured Property	Sensor Response or Sensitivity	Response/Recovery Time	Sensing Range	Hysteresis	Ref.
Alkaline treatment	Resistance	$(R_{dry} - R_{wet})/R_{dry} \times 100$ 99.7% (80% RH)	10/300 s	10–80% RH	8.8%	This work
Not Reduced	Resistance	$(R_{40\%RH} - R)/R_{40\%RH} \times 100$ 96.3% (80% RH)	Not given	40–80% RH	Not given	[13]
UV lamp irradiation	Resistance	R_{dry}/R_{wet} 15.0 (90% RH)	2.3/0.6 s	26–90% RH	Not given	[42]
Two-beam-laser interference	Impedance	Not give	3/10 s	11–95% RH	6.0%	[43]
Not reduced	Impedance	$(Z_{wet1} - Z_{wet2})/(RH_2 - RH_1)$ 33.3%	50/79 s	11–95% RH	Not given	[44]
$NaBH_4$	Impedance	logZ/%RH −0.0423	28/48 s	30–90% RH	2.5%	[45]

In present work, the particularly relevant hysteretic behavior can be explained considering that, in consequence of the alkaline treatment, a large fraction of ionized groups including $–COO^-$ and $–C–O^-$ was probably produced together with chemical reduction. These charged species could favor water molecules physisorption through electrostatic interactions and hinder and slow down water molecules desorbing. Consistently, Park et al. found increasing hysteresis values in GO films deposited from solutions with a respective increase of pH [46].

The sensor reliability was tested for six successive cycles at 6% RH and 60% RH as shown in Figure 9.

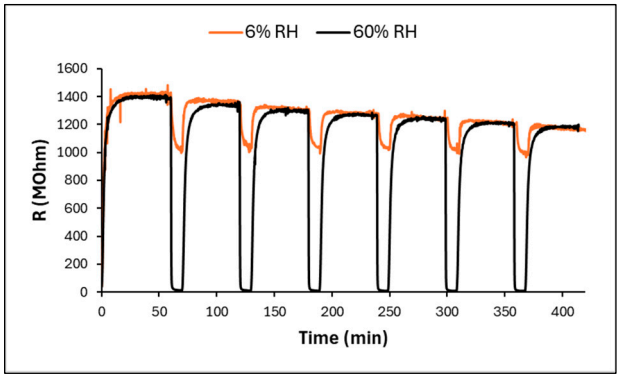

Figure 9. Six repeated cycles of sensor device exposed to 6% RH and 60% RH at room temperature.

The responses were very reproducible in time although also in this case the final resistance values were slightly lower than starting values. A baseline drift of 14% was observed in a total time of 6 h. During the desorption process, some water molecules can often remain on rGO surface or entrapped among rGO layers by chemical or physical adsorption, causing the partial recovery of initial state.

Repeated cycling test, performed in a period of six months attested a good term stability of rGO active layer, with a limited further decrease of the baseline resistances. In future, understanding the chemistry of rGO exposed to external stimuli such as light, humidity, or temperature will be crucial to tune rGO sensing properties such as long-term stability and repeatability.

3.3. Sensitivity Toward Volatile Organic Compounds

The gas sensing studies were completed considering the exposure effects to several common volatile organic compounds (VOCs) having different polarity such as ethanol, isopropanol, acetone, ethyl acetate, ethyl ether and petroleum ether. Typical signals recorded at 50% RH were reported in Figure 10.

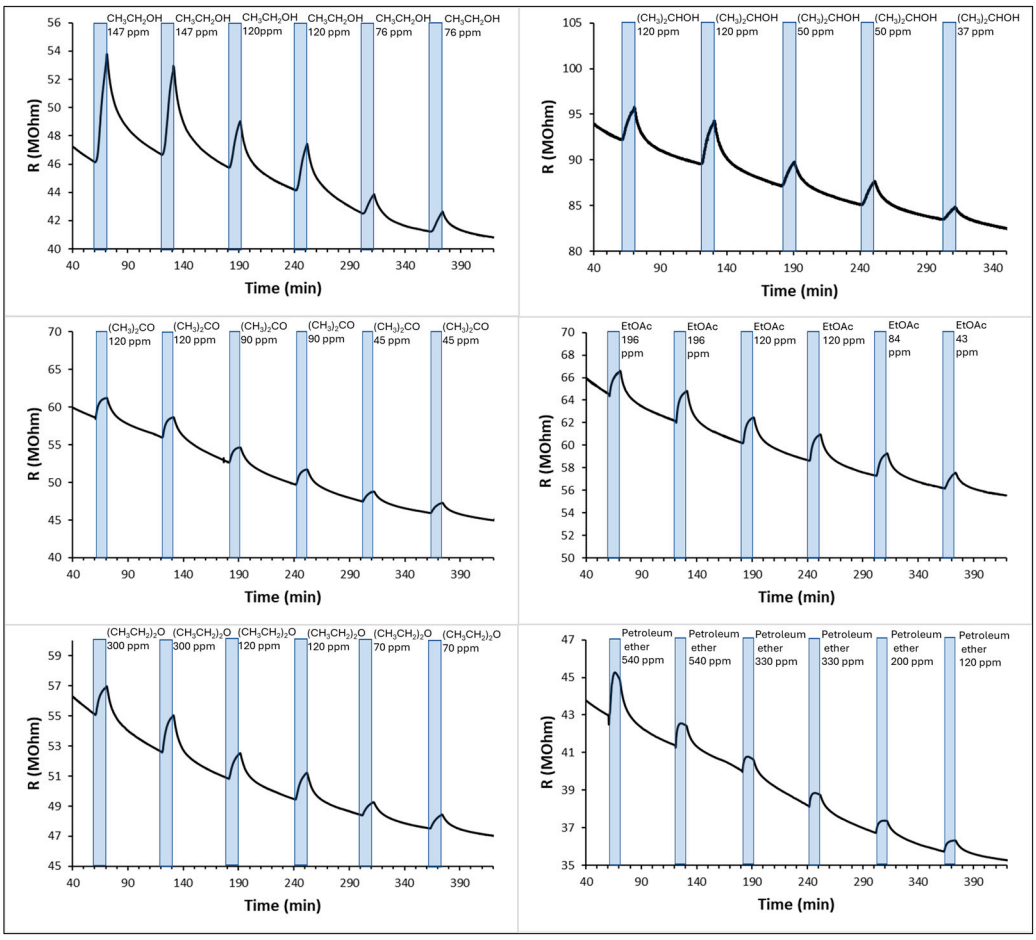

Figure 10. Sensor signals upon exposure to several concentrations of ethanol, isopropanol, ethyl acetate, ethyl ether and petroleum ether at 50% RH and room temperature.

Contrary to what was observed for water, exposure to VOCs induced an increase in electrical resistance. In this case, the organic vapors can partially replace the water molecules on the sensor surface, hindering the Grotthuss chain reaction. The average sensor responses (SR%), calculated at a VOC concentration of 120 ppm, were 11.3%, 10.3%, 3.8%, 3.7%, 3.4%, and 1.5% for ethanol, isopropanol, acetone, ethyl acetate, ethyl ether, and petroleum ether, respectively. As expected, the sensor responses decreased upon exposure to less polar molecules, and the alcoholic compounds can be considered the main interfering agents for the proposed humidity sensor.

4. Conclusions

In summary, using a rGO thin film as sensing material, we fabricated a chemiresistive flexible sensor useful to detect moisture in the wide range 10–80% RH. The rGO was produced in alkaline solution in relatively mild condition with the aim to improve electrical conductivity and, at the same time, to preserve most of the oxygenated functional groups on surface. Being rich in oxygenated moieties, such as hydroxyl and epoxy groups, the rGO can easily capture water molecules from the external environment. When water concentration is sufficiently high, the conductivity generated by the Grotthuss chain reaction induced a

rapid and drastic resistance decrease in rGO thin film. Remarkable sensor performances in terms of sensitivity and response time were measured.

The simple design, the excellent sensitivity at room temperature, the responses' repeatability, the wide RH range detected, and the fast response time are the main ad-vantages of the proposed humidity sensor. In addition, the flexibility, the easy fabrication process, the high elasticity, and the robustness make the device suitable for applications in many emerging areas, including wearable devices, structural health monitoring, portable consumer electronics, and robotic smart skin. The main drawbacks of the study are related to hysteretic behavior and an excessively long recovery time. In addition, after the recovery run, the resistance values were lower than the starting resistance, indicating an incomplete removal of water molecules from the sensing layer. Controlling the structure, chemical stability, and sensing properties of the rGO by choosing suitable procedures for synthesis, purification, and chemical reduction will be crucial to improving the performance of rGO-based sensor devices.

Author Contributions: Conceptualization, A.M.L. and M.P.; methodology, A.M.L., G.C. and M.P.; formal analysis, E.B. and M.L.P.; investigation, A.M.L., E.B. and M.L.P.; resources, G.C. and M.P.; data curation, A.M.L. and M.P.; writing—original draft preparation, A.M.L. and M.P.; writing-review and editing, A.M.L. and M.P.; supervision, A.M.L. and M.P. All authors have read and agreed to the published version of the manuscript.

Funding: This research received no external funding.

Institutional Review Board Statement: Not applicable.

Informed Consent Statement: Not applicable.

Data Availability Statement: All requested information will be provided by the corresponding author.

Acknowledgments: The authors would like to thank BIOAGE company for silver interdigitated electrodes fabrication by using photolithographic printing techniques.

Conflicts of Interest: The authors declare no conflicts of interest.

References

1. Delipinar, T.; Shafique, A.; Goahr, M.S.; Yapici, M.K. Fabrication and materials integration of flexible humidity sensors for emerging applications. *ACS Omega* **2021**, *6*, 8744–8753. [CrossRef] [PubMed]
2. Zang, D.; Wang, M.; Tang, M.; Song, X.; Zhang, X.; Kang, Z.; Liu, X.; Zhang, J.; Xue, Q. Recent progress of diversiform humidity sensors based on versatile nanomaterials and their prospective applications. *Nano Res.* **2022**, *16*, 11938–11958. [CrossRef]
3. Shaukat, R.A.; Tamim, A.M.; Hwang, G.T.; Jeong, C.K. Humidity sensors using 2D and 3D nanmoaterials: From materials selection to technological aspects. *Trans. Electr. Electron. Mater.* **2024**, *25*, 123–140. [CrossRef]
4. Mouhat, F.; Coudert, F.X.; Bocquet, M.L. Structure and chemistry of graphene oxide in liquid water from first principles. *Nat. Commun.* **2020**, *11*, 1566. [CrossRef]
5. Jung, I.; Dikin, D.; Park, S.; Cai, W.; Mielke, S.L.; Ruoff, R.S. Effect of water vapor on electrical properties of individual reduced graphene oxide sheets. *J. Phys. Chem. C* **2008**, *112*, 20264–20268. [CrossRef]
6. Jin, H.; Tao, X.; Feng, B.; Yu, L.; Wang, D.; Dong, S.; Luo, J. A humidity sensor based on quartz crystal microbalance using graphene oxide as a sensitive layer. *Vacuum* **2017**, *140*, 101–105. [CrossRef]
7. Yao, Y.; Chen, X.; Li, X.; Chen, X.; Li, N. Investigation of the stability of QCM humidity sensor using graphene oxide as sensing films. *Sens. Actuators B Chem.* **2014**, *191*, 779–783. [CrossRef]
8. Yao, Y.; Chen, X.; Guo, H.; Wu, Z. Graphene oxide thin film coated quartz crystal microbalance for humidity detection. *Appl. Surf. Sci.* **2011**, *257*, 7778–7782. [CrossRef]
9. Xuan, W.; He, M.; Meng, N.; He, X.; Wang, W.; Chen, J.; Shi, T.; Hasan, T.; Xu, Z.; Xu, Y.; et al. Fast response and high sensitivity ZnO/glass surface scoustic wave humidity sensors using graphene oxide sensing layer. *Sci. Rep.* **2014**, *4*, 4206. [CrossRef]
10. Balashov, S.M.; Balachova, O.V.; Filho, A.P.; Bazetto, M.C.Q.; de Almeida, M.G. Surface acoustic wave humidity sensors based on graphene oxide thin films deposited with the surface acoustic wave atomizer. *ECS Trans.* **2012**, *49*, 445–450. [CrossRef]
11. Bi, H.; Yin, K.; Xie, X.; Ji, J.; Wan, S.; Sun, L.; Terrones, M.; Dresselhaus, M.S. Ultrahigh humidity sensitivity of graphene oxide. *Sci. Rep.* **2013**, *3*, 2714. [CrossRef]
12. Yao, Y.; Chen, X.; Guo, H.; Wu, Z.; Li, X. Humidity sensing behaviors of graphene oxide-silicon bi-layer flexible structure. *Sens. Actuators B Chem.* **2012**, *161*, 1053–1058. [CrossRef]

13. Wang, C.; Cui, Z.; Zhu, Y.; Liu, X.; Wang, L.; Wang, L.J. Nanoarchitectonics of high-sensitivity humidity sensors based on graphene oxide films for respiratory monitoring. *Diam. Relat. Mater.* **2024**, *144*, 110970. [CrossRef]
14. Cai, J.; Lv, C.; Aoyagi, E.; Ogawa, S.; Watanabe, A. Laser direct writing of a high-performance all-graphene humidity sensor working in a novel sensing mode for portable electronics. *ACS Appl. Mater. Interfaces* **2018**, *10*, 23987–23996. [CrossRef] [PubMed]
15. Lei, D.; Zhang, Q.; Liu, N.; Su, T.; Wang, L.; Ren, Z.; Zhang, Z.; Su, J.; Gao, Y. Self-powered graphene oxide humidity sensor based on potentiometric humidity transduction mechanism. *Adv. Funct. Mater.* **2022**, *32*, 2107330. [CrossRef]
16. Zeng, S.; Pan, Q.; Huang, Z.; Gu, C.; Wang, T.; Xu, J.; Yan, Z.; Zhao, F.; Li, P.; Tu, Y.; et al. Ultrafast response of self-powered humidity sensor of flexible graphene oxide film. *Mater. Des.* **2023**, *226*, 111683. [CrossRef]
17. Zaharie-Butucel, D.; Digianantonio, L.; Leordean, C.; Ressier, L.; Astilean, S.; Farcau, C. Flexible transparent sensors from reduced graphene oxide microstripes fabricated by convective self-assembly. *Carbon* **2017**, *113*, 361–370. [CrossRef]
18. Phan, D.T.; Chung, G.S. Effects of rapid thermal annealing on humidity sensor based on graphene oxide thin films. *Sens. Actuators B Chem.* **2015**, *220*, 1050–1055. [CrossRef]
19. Becerril, H.A.; Mao, J.; Liu, Z.; Stoltenberg, R.M.; Bao, Z.; Chen, Y. Evaluation of solution-processed reduced graphene oxide films as transparent conductors. *ACS Nano* **2008**, *2*, 463–470. [CrossRef]
20. Laera, A.M.; Penza, M. Chemiresistive materials for alcohol vapor sensing at room temperature. *Chemosensors* **2024**, *12*, 78. [CrossRef]
21. Stankovich, S.; Dikin, D.A.; Piner, R.D.; Kohlhaas, K.A.; Kleinhammes, A.; Jia, Y.; Wu, Y.; Nguyen, S.T.; Ruoff, R.S. Synthesis of graphene-based nanosheets via chemical reduction of exfoliated graphite oxide. *Carbon* **2007**, *45*, 1558–1565. [CrossRef]
22. Chua, C.K.; Pumera, M. Reduction of graphene oxide with substituted borohydrides. *J. Mater. Chem. A* **2013**, *1*, 1892–1898. [CrossRef]
23. Song, P.; Zhang, X.; Sun, M.; Cui, X.; Lin, Y. Synthesis of graphene nanosheets via oxalic acid-induced chemical reduction of exfoliated graphite oxide. *RSC Adv.* **2012**, *2*, 1168–1173. [CrossRef]
24. Zhou, T.; Chen, F.; Tang, C.; Bai, H.; Zhang, Q.; Deng, H.; Fu, Q. The preparation of high performance and conductive poly (vinyl alcohol)/graphene nanocomposite via reducing graphite oxide with sodium hydrosulfite. *Compos. Sci. Technol.* **2011**, *71*, 1266–1270. [CrossRef]
25. Fan, X.; Peng, W.; Li, Y.; Li, X.; Wang, S.; Zhang, G.; Zhang, F. Deoxygenation of exfoliated graphite oxide under alkaline conditions: A green route to graphene preparation. *Adv. Mat.* **2008**, *20*, 4490–4493. [CrossRef]
26. Laera, A.M.; Cassano, G.; Burresi, E.; Protopapa, M.L.; Penza, M. A graphene oxide flexible sensor for humidity detection. *Eng. Proc.* **2023**, *48*, 44. [CrossRef]
27. Hummers, W.S.; Offeman, R.E. Preparation of graphene oxide. *J. Am. Chem. Soc.* **1958**, *80*, 1339. [CrossRef]
28. Taha, W.M.; Morsy, M.; Nada, N.A.; Ibrahim, M. Studying the humidity sensing behavior of MWCNTs boosted with Co_3O_4 nanorods. *Diam. Relat. Mater.* **2022**, *121*, 108754. [CrossRef]
29. Liu, M.Q.; Wang, C.; Kim, N.Y. High-sensitivity and low-hysteresis porous MIM-type capacitive humidity sensor using functional polymer mixed with TiO_2 microparticles. *Sensors* **2017**, *17*, 284. [CrossRef]
30. Zu, Y.; Duan, Z.; Yuan, Z.; Jiang, Y.; Tai, H. Electrospun nanofiber-based humidity sensors: Materials, devices, and emerging applications. *J. Mater. Chem. A.* **2024**, *12*, 27157. [CrossRef]
31. Kudin, K.N.; Ozbas, B.; Schniepp, H.C.; Prud'Homme, R.K.; Aksay, I.A.; Car, R. Raman spectra of graphite oxide and functionalized graphene sheets. *Nano Lett.* **2008**, *8*, 36–41. [CrossRef] [PubMed]
32. Shin, H.J.; Kim, K.K.; Benayad, A.; Yoon, S.M.; Park, H.K.; Jung, I.S.; Jin, M.H.; Jeong, H.K.; Kim, J.M.; Choi, J.Y. Efficient reduction of graphite oxide by sodium borohydride and its effect on electrical conductance. *Adv. Funct. Mater.* **2009**, *19*, 1987–1992. [CrossRef]
33. Yang, S.; Yue, W.; Huang, D.; Chen, C.; Lin, H.; Yang, X. A facile green strategy for rapid reduction of graphene oxide by metallic zinc. *RSC Adv.* **2012**, *2*, 8827–8832. [CrossRef]
34. Yan, J.A.; Xian, L.; Chou, M.Y. Structural and electronic properties of oxidized graphene. *Phys. Rev. Lett.* **2009**, *103*, 086802. [CrossRef]
35. Chien, C.T.; Li, S.S.; Lai, W.J.; Yeh, Y.C.; Chen, H.A.; Chen, I.S.; Chen, L.C.; Chen, K.H.; Nemoto, T.; Isoda, S.; et al. Tunable photoluminescence from graphene oxide. *Angew. Chem. Int. Ed.* **2012**, *51*, 6662–6666. [CrossRef]
36. Eda, G.; Lin, Y.Y.; Mattevi, C.; Yamaguchi, H.; Chen, H.A.; Chen, I.S.; Chen, C.W.; Chhowalla, M. Blue photoluminescence from chemically derived graphene oxide. *Adv. Mater.* **2010**, *22*, 505–509. [CrossRef]
37. Cerveny, S.; Barroso-Bujans, F.; Alegria, A.; Colmenero, J. Dynamics of water intercalated in graphite oxide. *J. Phys. Chem. C* **2010**, *114*, 2604–2612. [CrossRef]
38. Gao, W.; Singh, N.; Song, L.; Liu, Z.; Reddy, A.L.M.; Ci, L.; Vajtai, R.; Zhang, Q.; Wei, B.; Ajayan, P.M. Direct laser writing of micro-supercapacitors on hydrated graphite oxide films. *Nat. Nanotechnol.* **2011**, *6*, 496–500. [CrossRef]
39. David, R.; Kumar, R. Reactive events at the graphene oxide-water interface. *Chem. Comm.* **2021**, *57*, 11697–11700. [CrossRef]
40. Smith, A.D.; Elgammal, K.; Niklaus, F.; Delin, A.; Fischer, A.C.; Vaziri, S.; Forsberg, F.; Rasander, M.; Hugosson, H.; Bergqvist, L.; et al. Resistive graphene humidity sensors with rapid and direct electrical readout. *Nanoscale* **2015**, *7*, 19099. [CrossRef]
41. Shooshtari, M.; Salehi, A.; Vollebregt, S. Effect of humidity on gas sensing performance of carbon nanotube gas sensors operated at room temperature. *IEEE Sens. J.* **2021**, *21*, 5763–5770. [CrossRef]

42. Ranjan, P.; Tiwary, P.; Chakraborty, A.K.; Mahapatra, R.; Thakur, A.D. Graphene oxide based free-standing films for humidity and hydrogen peroxide sensing. *J. Mater. Sci. Mater. Electron.* **2018**, *29*, 15946–15956. [CrossRef]
43. Guo, L.; Jiang, H.B.; Shao, R.Q.; Zhang, Y.L.; Xie, S.Y.; Wang, J.N.; Li, X.B.; Jiang, F.; Chen, Q.D.; Zhang, T.; et al. Two-beam-laser interference mediated reduction, patterning and nanostructuring of graphene oxide for the production of a flexible humidity sensing device. *Carbon* **2012**, *50*, 1667–1673. [CrossRef]
44. Feng, X.; Chen, W.; Yan, L. Free-standing dried foam films of graphene oxide for humiditysensing. *Sens. Actuators B Chem.* **2015**, *215*, 316–322. [CrossRef]
45. Su, P.G.; Chiou, C.F. Electrical and humidity-sensing properties of reduced graphene oxidethin film fabricated by layer-by-layer with covalent anchoring onflexible substrate. *Sens. Actuators B Chem.* **2014**, *200*, 9–18. [CrossRef]
46. Park, E.U.; Choi, B.I.; Kim, J.C.; Woo, S.B.; Kim, Y.G.; Choi, Y.; Lee, S.W. Correlation between the sensitivity and the hysteresis of humidity sensors based on graphene oxides. *Sens. Actuators B Chem.* **2018**, *258*, 255–262. [CrossRef]